

## New Theoretical Results on Event-by-Event Fluctuations

---

**Mark I. Gorenstein\***

*Bogolyubov Institute for Theoretical Physics, Kiev, Ukraine*

*E-mail: goren@bitp.kiev.ua*

Several theoretical results concerning event-by-event fluctuations are discussed:

- (1) a role of the global conservation laws and concept of statistical ensembles;
- (2) strongly intensive measures for physical systems with volume fluctuations;
- (3) identity method for chemical fluctuations in a case of incomplete particle identification;
- (4) the example of particle number fluctuations in a vicinity of the critical point.

*9th International Workshop on Critical Point and Onset of Deconfinement - CPOD2014,  
17-21 November 2014*

*ZiF (Center of Interdisciplinary Research)  
, University of Bielefeld, Germany*

---

\*Speaker.

## 1. Introduction

The study of event-by-event (e-by-e) fluctuations in high-energy nucleus-nucleus (A+A) collisions opens new possibilities to investigate properties of strongly interacting matter (see, e.g., Refs. [1] and [2] and references therein). Specific fluctuations can signal the onset of deconfinement when the collision energy becomes sufficiently high to create the quark-gluon plasma (QGP) at the initial stage of A+A collision [3, 4]. By measuring the fluctuations, one may also observe effects caused by the dynamical instabilities when the expanding system goes through the 1<sup>st</sup> order transition line between the QGP and the hadron resonance gas [5]. Furthermore, the critical point (CP) of strongly interacting matter may be signaled by characteristic fluctuation pattern [6, 7, 8]. Therefore, e-by-e fluctuations are an important tool for the study of properties of the onset of deconfinement and the search for the CP of strongly interacting matter. However, mostly due to the incomplete acceptance of detectors, difficulties to control e-by-e the number of interacting nucleons, and also not well adapted data analysis tools, the results on e-by-e fluctuations are not yet mature. Even the simplest tests of statistical and dynamical models at the level of fluctuations are still missing.

In this presentation the theoretical progress in several areas related to the study of e-by-e fluctuations is reported. A role of the global conservation laws is discussed in Sec. 2. The strongly intensive measures of e-by-e fluctuations are introduced in Sec. 3. They give a possibility to study e-by-e fluctuations in a physical system when its average size and size fluctuations can not be controlled experimentally. In Sec. 4 a novel procedure, the identity method, is described for analyzing fluctuations of identified hadrons under typical experimental conditions of incomplete particle identification. Finally, in Sec. 5 using the van der Waals equation of state adopted to the grand canonical ensemble formulation we discuss particle number fluctuations in a vicinity of the CP. Most part of our discussion concerns the e-by-e fluctuations of hadron multiplicities. However, many of our physical conclusions can be applied to more general cases.

## 2. Global Conservations Laws

In this section we illustrate the role of global conservation laws in calculating of e-by-e fluctuations within statistical mechanics. Successful applications of the statistical model to description of mean hadron multiplicities in high energy collisions (see, e.g., Refs. [9, 10, 11] and references therein) has stimulated investigations of properties of the statistical ensembles. Whenever possible, one prefers to use the grand canonical ensemble (GCE) due to its mathematical convenience. The canonical ensemble (CE) should be applied [12, 13] when the number of carriers of conserved charges is small (of the order of 1), such as strange hadrons [14], antibaryons [15], or charmed hadrons [16]. The micro-canonical ensemble (MCE) has been used [17, 18, 19] to describe small systems with fixed energy, e.g., mean hadron multiplicities in proton-antiproton annihilation at rest. In all these cases, calculations performed in different statistical ensembles yield different results. This happens because the systems are ‘small’ and they are ‘far away’ from the thermodynamic limit (TL). The multiplicities of hadrons produced in relativistic heavy ion collisions are typically much larger than 1. Thus, their mean values obtained within GCE, CE, and MCE approach each

other. One refers here to the thermodynamical equivalence of statistical ensembles in the TL and uses the GCE, as a most convenient one, for calculating the hadron yields.

A statistical system is characterized by the extensive quantities: volume  $V$ , energy  $E$ , and conserved charge(s)<sup>1</sup>  $Q$ . The MCE is defined by the postulate that all micro-states with given  $V$ ,  $E$ , and  $Q$  have equal probabilities of being realized. This is the basic postulate of statistical mechanics. The MCE partition function just calculates the number of microscopic states with given fixed  $(V, E, Q)$  values. In the CE the energy exchange between the considered system and ‘infinite thermal bath’ is assumed. Consequently, a new parameter, temperature  $T$ , is introduced. To define the GCE, one makes a similar construction for the conserved charge  $Q$ : an ‘infinite chemical bath’ and the chemical potential  $\mu$  are introduced. The CE introduces the energy fluctuations. In the GCE, there are additionally the charge fluctuations. Therefore, the global conservation laws of  $E$  and  $Q$  are treated in different ways: in the MCE both  $E$  and  $Q$  are fixed in each microscopic state, whereas only average value of  $E$  is fixed in the CE, and average values of  $E$  and  $Q$  in the GCE.

The MCE, CE, and GCE are the most familiar statistical ensembles. In several textbooks (see, e.g., Ref. [20, 21]), the pressure (or isobaric) ensemble has been also discussed. An ‘infinite bath of the fixed external pressure’  $p$  is then introduced. This leads to volume fluctuations around the average value (see Ref. [22]). In general, there are 3 pairs of variables –  $(V, p)$ ,  $(E, T)$ ,  $(Q, \mu)$  – and, thus, the 8 statistical ensembles<sup>2</sup> can be constructed.

Measurements of hadron multiplicity distributions in A+A collisions, open a new field of applications of the statistical models. The particle multiplicity fluctuations are usually quantified by a ratio of the variance to mean value, the scaled variance,

$$\omega[N] \equiv \frac{\langle N^2 \rangle - \langle N \rangle^2}{\langle N \rangle}, \quad (2.1)$$

and are a subject of current experimental activities. In statistical models there is a qualitative difference in properties of a mean multiplicity and a scaled variance of multiplicity distribution. It was recently found [23, 24, 25, 26, 27, 28, 29, 30, 31, 32, 33, 34] that even in the TL corresponding results for the scaled variance are different in different ensembles. Hence the equivalence of ensembles holds for mean values in the TL, but does not extend to fluctuations. Several examples below illustrate this statement.

## 2.1 Canonical Ensemble

Let us consider a system which consists of one sort of positively +1 and negatively -1 charged particles (e.g.,  $\pi^+$  and  $\pi^-$  mesons) with total charge equal to zero  $Q = 0$ . For the relativistic Boltzmann ideal gas in the volume  $V$  at temperature  $T$  the GCE partition function reads:

$$Z_{\text{gce}}(V, T) = \sum_{N_+=0}^{\infty} \sum_{N_-=0}^{\infty} \frac{(\lambda_+ z)^{N_+}}{N_+!} \frac{(\lambda_- z)^{N_-}}{N_-!} = \exp(\lambda_+ z + \lambda_- z) = \exp(2z). \quad (2.2)$$

<sup>1</sup>These conserved charges are usually the net baryon number, strangeness, and electric charge. In non-relativistic statistical mechanics the number of particles plays the role of a conserved ‘charge’.

<sup>2</sup>For several conserved charges  $\{Q_i\}$  the number of possible ensembles is larger, as each charge can be treated either canonically or grand canonically.

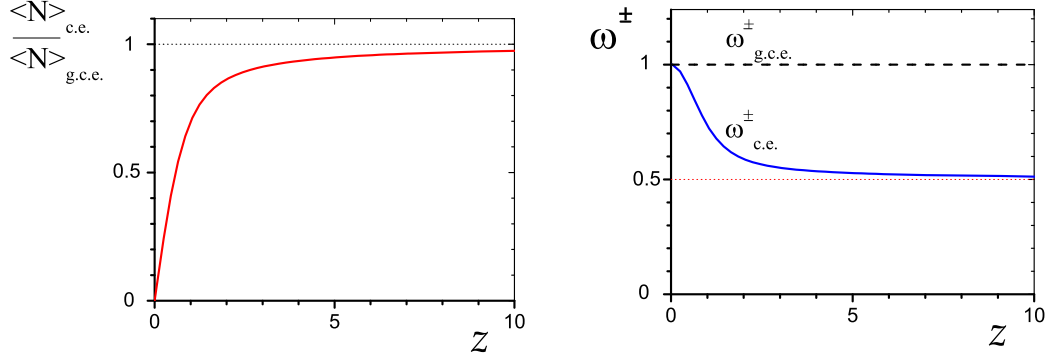


**Figure 1:** *Left:* The ratio of  $\langle N_{\pm} \rangle_{\text{ce}}$  (2.6) to  $\langle N_{\pm} \rangle_{\text{gce}}$  (2.5) as a function of  $z$ . *Right:* The scaled variances of  $N_{\pm}$  calculated within the GCE,  $\omega_{\text{gce}}^{\pm} = 1$  (2.7), and CE,  $\omega_{\text{c.e.}}^{\pm}$  (2.8).

In Eq. (2.2)  $z$  is a single particle partition function

$$z = \frac{V}{2\pi^2} \int_0^{\infty} k^2 dk \exp \left[ -\frac{(k^2 + m^2)^{1/2}}{T} \right] = \frac{V}{2\pi^2} T m^2 K_2 \left( \frac{m}{T} \right), \quad (2.3)$$

where  $m$  is a particle mass, and  $K_2$  is the modified Hankel function. Parameters  $\lambda_+$  and  $\lambda_-$  are auxiliary parameters introduced in order to calculate mean numbers and fluctuations of the positively and negatively charged particles. They are set to one in the final formulas. The chemical potential equals zero to satisfy the condition  $\langle Q \rangle_{\text{gce}} = 0$ .

The CE partition function is obtained by an explicit introduction of the charge conservation constrain,  $Q = N_+ - N_- = 0$ , for each microscopic state of the system and it reads:

$$\begin{aligned} Z_{\text{ce}}(V, T) &= \sum_{N_+=0}^{\infty} \sum_{N_-=0}^{\infty} \frac{(\lambda_+ z)^{N_+}}{N_+!} \frac{(\lambda_- z)^{N_-}}{N_-!} \delta(N_+ - N_-) = \\ &= \frac{1}{2\pi} \int_0^{2\pi} d\phi \exp [z (\lambda_+ e^{i\phi} + \lambda_- e^{-i\phi})] = I_0(2z), \end{aligned} \quad (2.4)$$

where the integral representations of the  $\delta$ -Kronecker symbol and the modified Bessel function  $I_0$  were used. The average number of  $N_+$  and  $N_-$  can be calculated as [35]:

$$\langle N_{\pm} \rangle_{\text{gce}} = \left( \frac{\partial}{\partial \lambda_{\pm}} \ln Z_{\text{gce}} \right)_{\lambda_{\pm}=1} = z. \quad (2.5)$$

$$\langle N_{\pm} \rangle_{\text{ce}} = \left( \frac{\partial}{\partial \lambda_{\pm}} \ln Z_{\text{ce}} \right)_{\lambda_{\pm}=1} = z \frac{I_1(2z)}{I_0(2z)}. \quad (2.6)$$

The exact charge conservation leads to the CE suppression,  $I_1(2z)/I_0(2z) < 1$ , of the charged particle multiplicities relative to the results for the GCE (2.5). The ratio of  $\langle N_{\pm} \rangle$  calculated in the CE and GCE is plotted as a function of  $z$  in Fig. 1 *left*.

The corresponding scaled variances are [23]:

$$\omega_{\text{gce}}^{\pm} = \frac{\langle N_{\pm}^2 \rangle_{\text{gce}} - \langle N_{\pm} \rangle_{\text{gce}}^2}{\langle N_{\pm} \rangle_{\text{gce}}} = 1, \quad (2.7)$$

$$\omega_{\text{ce}}^{\pm} = \frac{\langle N_{\pm}^2 \rangle_{\text{ce}} - \langle N_{\pm} \rangle_{\text{ce}}^2}{\langle N_{\pm} \rangle_{\text{ce}}} = 1 - z \left[ \frac{I_1(2z)}{I_0(2z)} - \frac{I_2(2z)}{I_1(2z)} \right]. \quad (2.8)$$

In the large volume limit ( $V \rightarrow \infty$  corresponds also to  $z \rightarrow \infty$ ) one can use an asymptotic expansion of the modified Bessel function,

$$\lim_{z \rightarrow \infty} I_n(2z) = \frac{\exp(2z)}{\sqrt{4\pi z}} \left[ 1 - \frac{4n^2 - 1}{16z} + O\left(\frac{1}{z^2}\right) \right], \quad (2.9)$$

and obtains:

$$\langle N_{\pm} \rangle_{\text{ce}} \cong \langle N_{\pm} \rangle_{\text{g.c.e}} = z, \quad (2.10)$$

$$\omega_{\text{ce}}^{\pm} \cong \frac{1}{2} + \frac{1}{8z} \cong \frac{1}{2} = \frac{1}{2} \omega_{\text{gce}}^{\pm}. \quad (2.11)$$

The dependence of the scaled variance calculated within the CE and GCE on  $z$  is shown in Fig. 1 *right*. The scaled variance shows a very different behavior than the mean multiplicity: in the large  $z$  limit the mean multiplicity ratio approaches one and the scaled variance ratio 1/2. Thus, in the case of  $N_{\pm}$  fluctuations the CE and GCE are not equivalent.

## 2.2 Micro-Canonical Ensemble

Our second example is the ideal gas of massless neutral Boltzmann particles. We consider the same volume and energy in the MCE and GCE and compare these to formulations. The fixed MCE energy  $E$  and the mean GCE energy  $\langle E \rangle_{\text{gce}}$  are connected via equation (the degeneracy factor is  $g = 1$ ):

$$E = \langle E \rangle_{\text{gce}} = \frac{3}{\pi^2} V T^4. \quad (2.12)$$

The mean multiplicity  $\langle N \rangle_{\text{mce}}$  in the MCE is approximately equal to the GCE value:

$$\langle N \rangle_{\text{mce}} \cong \langle N \rangle_{\text{gce}} = \frac{1}{\pi^2} V T^3 \equiv \bar{N}. \quad (2.13)$$

The approximation  $\langle N \rangle_{\text{mce}} \cong \bar{N}$  is valid for  $\bar{N} \gg 1$  and reflects the thermodynamic equivalence of the MCE and GCE. The scaled variances for the multiplicity fluctuations are, however, different in the GCE and MCE [29]:

$$\omega_{\text{gce}} = \frac{\langle N^2 \rangle_{\text{gce}} - \langle N \rangle_{\text{gce}}^2}{\langle N \rangle_{\text{gce}}} = 1, \quad (2.14)$$

$$\omega_{\text{mce}} = \frac{\langle N^2 \rangle_{\text{mce}} - \langle N \rangle_{\text{mce}}^2}{\langle N \rangle_{\text{mce}}} = \frac{1}{4}. \quad (2.15)$$

Thus, despite of thermodynamic equivalence of the MCE and GCE the value of  $\omega_{\text{mce}}$  is four times smaller than the scaled variance of the GCE (Poisson) distribution,  $\omega_{\text{gce}} = 1$ . Figure 2(a) shows a

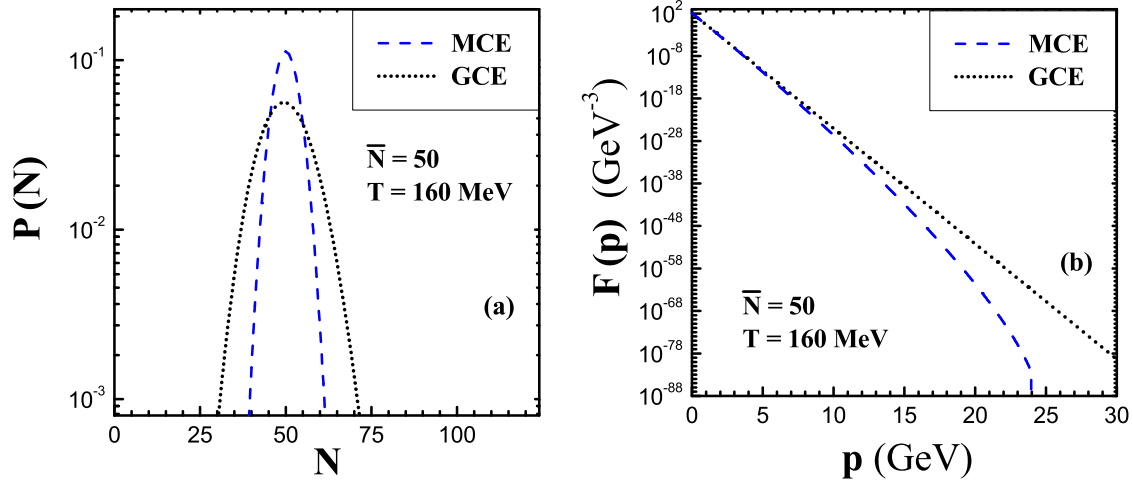


**Figure 2:** (a): The multiplicity distribution  $P(N)$  of massless neutral particles in the MCE, dashed line, and the GCE (Poisson) distribution, dotted line, for the same mean multiplicity,  $\bar{N} = 50$ . (b): The momentum spectrum of massless neutral particles calculated within the MCE, dashed line, and the GCE (2.16), dotted line. The temperature is fixed as  $T = 160$  MeV and the system energy is  $E = 3\bar{N}T = 24$  GeV for both plots.

comparison of the MCE and GCE results for the multiplicity distributions  $P(N)$ . Different values of the scaled variances (2.14) and (2.15) signify the different widths of  $P(N)$  distributions in the GCE and MCE clearly seen in Fig. 2.

Figure 2(b) shows the single particle momentum spectra  $F(p)$  in the GCE and MCE ( $\bar{N} = 50$  and  $T = 160$  MeV). A single particle momentum spectrum in the GCE reads:

$$F_{\text{gce}}(p) \equiv \frac{1}{\bar{N}} \frac{dN}{p^2 dp} = \frac{V}{2\pi^2 \bar{N}} \exp\left(-\frac{p}{T}\right) = \frac{1}{2T^3} \exp\left(-\frac{p}{T}\right). \quad (2.16)$$

The MCE spectrum is very close to the Boltzmann distribution (2.16) at all momenta up to 10 GeV/c. At this momentum, the spectrum  $F(p)$  is already dropped in a comparison to its  $F(0)$  value by about a factor of  $10^{-30}$ . The MCE spectrum decreases faster than the GCE one at high momenta. Close to the threshold momentum,  $p = E = 24$  GeV, where the MCE spectrum goes to zero, large deviations from (2.16) are observed. In order to demonstrate these deviations the MCE and GCE momentum spectra are shown in Fig. 2 (b) over 90 orders of magnitude.

### 2.3 Hadron Resonance Gas in GCE, CE, and MCE

We present now the results of the hadron resonance gas (HRG) for the e-by-e fluctuations of negatively charged and positively charged hadrons (see details in Ref. [32]). The corresponding scaled variances  $\omega^-$  and  $\omega^+$  are calculated in the GCE, CE, and MCE along the chemical freeze-out line in central Pb+Pb (Au+Au) collisions for the whole energy range from SIS to LHC. The model parameters are the volume  $V$ , temperature  $T$ , baryonic chemical potential  $\mu_B$ , and the strangeness saturation parameter  $\gamma_S$ . They are chosen by fitting the mean hadron multiplicities. Once a suitable set of the chemical freeze-out parameters is determined for each collision energy, the scaled variances  $\omega^-$  and  $\omega^+$  can be calculated in different statistical ensembles. The results for the GCE, CE, and MCE are presented in Fig. 3 as functions of the center-of-mass energy  $\sqrt{s_{NN}}$

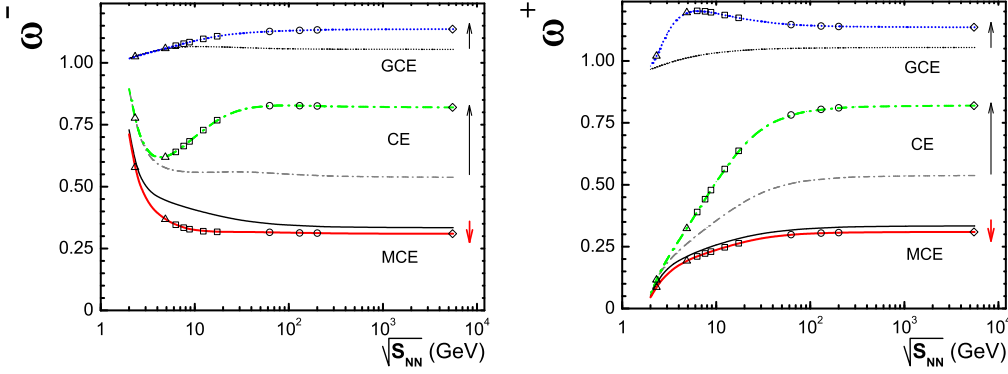


**Figure 3:** The scaled variances  $\omega^-$  (left) and  $\omega^+$  (right), both primordial and final, along the chemical freeze-out line for central Pb+Pb (Au+Au) collisions. Different lines present the GCE, CE, and MCE results. Symbols at the curves for final particles correspond to the specific collision energies. The arrows show the effect of resonance decays.

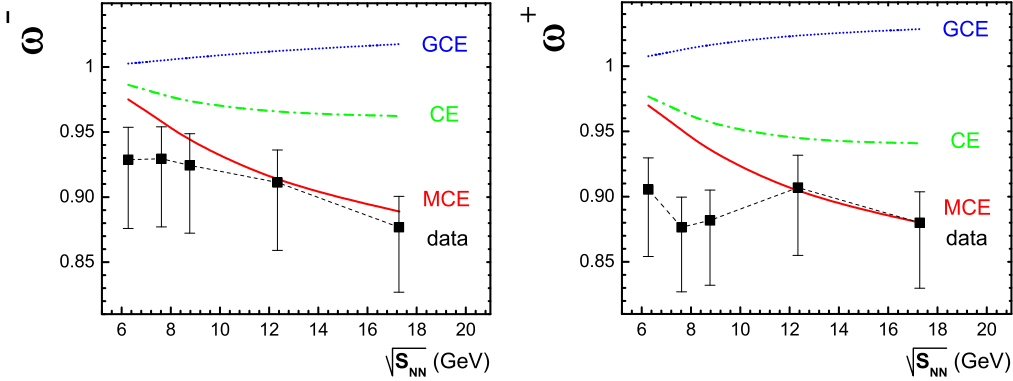


**Figure 4:** The scaled variance for negatively charged (left) and positively charged (right) hadrons along the chemical freeze-out line for central Pb+Pb collisions at the SPS energies. The points show the data of the NA49 Collaboration [36]. Curves show the GCE, CE, and MCE results calculated with the NA49 acceptance.

of the nucleon pair. A comparison between the data and predictions of statistical models should be performed for results which correspond to A+A collisions with a fixed number of nucleon participants. In Fig. 4 our statistical model results are compared with the NA49 data [36] at collision energies 20, 30, 40, 80 and 158 A GeV for the 1% most central Pb+Pb collisions selected by the numbers of projectile participants. In the experimental study of A+A collisions at high energies only a fraction of all produced particles is registered. If detected particles are uncorrelated, the scaled variance for the accepted particles,  $\omega_{\text{acc}}[N]$ , can be presented in terms of the full  $4\pi$  scaled variance  $\omega[N]$  as (see, e.g., [32])

$$\omega_{\text{acc}}[N] = 1 - q + q\omega[N], \quad (2.17)$$

where  $q$  is a probability of a single particle to be accepted. Figure 4 demonstrates that among three different statistical ensembles the MCE is in a better agreement with the NA49 data. The reasons of this are not yet clear.



## 2.4 Generalized Statistical Ensembles

A choice of statistical ensemble is crucial in calculating fluctuations. On the other hand, it is clear that GCE, CE, and MCE are only some typical examples. A general concept of the statistical ensembles was suggested in Ref. [37]. The extensive quantities  $(V, E, Q) \equiv \vec{A}$  define the MCE. Different statistical ensembles are then constructed using externally given distributions of extensive quantities,  $P_\alpha(\vec{A})$ . The distribution of any observable  $O$  in is then obtained in two steps. Firstly, the MCE  $O$ -distribution,  $P_{mce}(O; \vec{A})$ , is calculated at fixed values of the extensive quantities  $\vec{A}$ . Secondly, this result is averaged over the external distribution  $P_\alpha(\vec{A})$  [37]:

$$P_\alpha(O) = \int d\vec{A} P_\alpha(\vec{A}) P_{mce}(O; \vec{A}) . \quad (2.18)$$

Fluctuations of extensive quantities  $\vec{A}$  around their average values depend not on the system's physical properties, but rather on external conditions. One can imagine a huge variety of these conditions, thus, the standard statistical ensembles discussed above are only some special examples. The ensemble defined by Eq. (2.18), the  $\alpha$ -ensemble, includes the standard statistical ensembles as the particular cases. The generalized statistical mechanics based on Eq. (2.18) can be applied to different tasks of hadron production in high energy collisions. For example, based on Eq. (2.18) and introducing the scaling volume fluctuations  $P_\alpha(V)$ , an attempt was made in Ref. [38] to extend the statistical model to the hard domain of high transverse momenta and/or high hadron masses.

## 3. Strongly Intensive Measures of E-by-E Fluctuations

A significant increase of transverse momentum and multiplicity fluctuations is expected in the vicinity of the CP. One can probe different regions of the phase diagram by varying the collision energy and the size of colliding nuclei. The possibility to observe signatures of the critical point inspired the energy and system size scan program of the NA61/SHINE Collaboration at the CERN SPS [39] and the low beam energy scan program of the STAR and PHENIX Collaborations at the BNL RHIC [40]. In these studies one measures and then compares e-by-e fluctuations in collisions of different nuclei at different collision energies. The average sizes of the created physical systems and their e-by-e fluctuations are expected to be rather different (see, e.g., Ref. [41]). This strongly affects the observed fluctuations, i.e., the measured quantities would not describe the local physical properties of the system but rather reflect the system size fluctuations. For instance, A+A collisions with different centralities may produce a system with approximately the same local properties (e.g., the same temperature and baryonic chemical potential) but with the volume changing significantly from interaction to interaction. Note that in high energy collisions the average volume of created matter and its variations from collision to collision usually cannot be controlled experimentally. Therefore, a suitable choice of statistical tools for the study of e-by-e fluctuations is really important.

Intensive quantities are defined within the GCE of statistical mechanics. They depend on temperature and chemical potential(s), but they are independent of the system volume. Strongly intensive quantities introduced in Ref. [42] are, in addition, independent of volume fluctuations. They are the appropriate measures for studies of e-by-e fluctuations in A+A collisions and can be defined for two extensive state quantities  $A$  and  $B$ . Here, we call  $A$  and  $B$  *extensive* when the first



moments of their distributions for the ensemble of possible states are proportional to volume. They are referred to as *state quantities* as they characterize the states of the considered system, e.g., final states of A+A collisions or micro-states of the GCE.

There are two families of strongly intensive quantities which depend on the second and first moments of  $A$  and  $B$  and thus allow to study e-by-e (or state-by-state) fluctuations [42]:

$$\Delta[A, B] = \frac{1}{C_\Delta} \left[ \langle B \rangle \omega[A] - \langle A \rangle \omega[B] \right], \quad (3.1)$$

$$\Sigma[A, B] = \frac{1}{C_\Sigma} \left[ \langle B \rangle \omega[A] + \langle A \rangle \omega[B] - 2(\langle AB \rangle - \langle A \rangle \langle B \rangle) \right], \quad (3.2)$$

where

$$\omega[A] \equiv \frac{\langle A^2 \rangle - \langle A \rangle^2}{\langle A \rangle}, \quad \omega[B] \equiv \frac{\langle B^2 \rangle - \langle B \rangle^2}{\langle B \rangle}, \quad (3.3)$$

and averaging  $\langle \dots \rangle$  is performed over the ensemble of multi-particle states. The normalization factors  $C_\Delta$  and  $C_\Sigma$  are required to be proportional to the first moments of any extensive quantities.

In Ref. [43] a specific choice of the  $C_\Delta$  and  $C_\Sigma$  normalization factors was proposed. It makes the quantities  $\Delta[A, B]$  and  $\Sigma[A, B]$  dimensionless and leads to  $\Delta[A, B] = \Sigma[A, B] = 1$  in the independent particle model, as will be shown below.

From the definition of  $\Delta[A, B]$  and  $\Sigma[A, B]$  it follows that  $\Delta[A, B] = \Sigma[A, B] = 0$  in the case of absence of fluctuations of  $A$  and  $B$ , i.e., for  $\omega[A] = \omega[B] = \langle AB \rangle - \langle A \rangle \langle B \rangle = 0$ . Thus the proposed normalization of  $\Delta[A, B]$  and  $\Sigma[A, B]$  leads to a common scale on which the values of the fluctuation measures calculated for different state quantities  $A$  and  $B$  can be compared.

There is an important difference between the  $\Sigma[A, B]$  and  $\Delta[A, B]$  quantities. Namely, in order to calculate  $\Delta[A, B]$  one needs to measure only the first two moments:  $\langle A \rangle$ ,  $\langle B \rangle$  and  $\langle A^2 \rangle$ ,  $\langle B^2 \rangle$ . This can be done by independent measurements of the distributions  $P_A(A)$  and  $P_B(B)$ . The quantity  $\Sigma[A, B]$  includes the correlation term,  $\langle AB \rangle - \langle A \rangle \langle B \rangle$ , and thus requires, in addition, simultaneous measurements of  $A$  and  $B$  in order to obtain the joint distribution  $P_{AB}(A, B)$ .

### 3.1 $\Delta$ and $\Sigma$ in the Independent Particle Model

The IPM assumes that:

- (1) the state quantities  $A$  and  $B$  can be expressed as

$$A = \alpha_1 + \alpha_2 + \dots + \alpha_N, \quad B = \beta_1 + \beta_2 + \dots + \beta_N, \quad (3.4)$$

where  $\alpha_j$  and  $\beta_j$  denote single particle contributions to  $A$  and  $B$ , respectively, and  $N$  is the number of particles;

- (2) inter-particle correlations are absent, i.e., the probability of any multi-particle state is the product of probability distributions  $P(\alpha_j, \beta_j)$  of single-particle states, and these probability distributions are the same for all  $j = 1, \dots, N$  and independent of  $N$ ,

$$P_N(\alpha_1, \beta_1, \alpha_2, \beta_2, \dots, \alpha_N, \beta_N) = \mathcal{P}(N) \times P(\alpha_1, \beta_1) \times P(\alpha_2, \beta_2) \times \dots \times P(\alpha_N, \beta_N), \quad (3.5)$$

where  $\mathcal{P}(N)$  is an arbitrary multiplicity distribution of particles.

It can be shown [43] that within the IPM the average values of the first and second moments of  $A$  and  $B$  are equal to:

$$\langle A \rangle = \overline{\alpha} \langle N \rangle, \quad \langle A^2 \rangle = \overline{\alpha^2} \langle N \rangle + \overline{\alpha}^2 [\langle N^2 \rangle - \langle N \rangle], \quad (3.6)$$

$$\langle B \rangle = \overline{\beta} \langle N \rangle, \quad \langle B^2 \rangle = \overline{\beta^2} \langle N \rangle + \overline{\beta}^2 [\langle N^2 \rangle - \langle N \rangle], \quad (3.7)$$

$$\langle AB \rangle = \overline{\alpha\beta} \langle N \rangle + \overline{\alpha} \cdot \overline{\beta} [\langle N^2 \rangle - \langle N \rangle]. \quad (3.8)$$

The values of  $\langle A \rangle$  and  $\langle B \rangle$  are proportional to the average number of particles  $\langle N \rangle$  and, thus, to the average size of the system. These quantities are extensive. The quantities  $\overline{\alpha}$ ,  $\overline{\beta}$  and  $\overline{\alpha^2}$ ,  $\overline{\beta^2}$ ,  $\overline{\alpha\beta}$  are the first and second moments of the single-particle distribution  $P(\alpha, \beta)$ . Within the IPM they are independent of  $\langle N \rangle$  and play the role of intensive quantities.

Using Eq. (3.6) the scaled variance  $\omega[A]$  which describes the state-by-state fluctuations of  $A$  can be expressed as:

$$\omega[A] \equiv \frac{\langle A^2 \rangle - \langle A \rangle^2}{\langle A \rangle} = \frac{\overline{\alpha^2} - \overline{\alpha}^2}{\overline{\alpha}} + \overline{\alpha} \frac{\langle N^2 \rangle - \langle N \rangle^2}{\langle N \rangle} \equiv \omega[\alpha] + \overline{\alpha} \omega[N], \quad (3.9)$$

where  $\omega[\alpha]$  is the scaled variance of the single-particle quantity  $\alpha$ , and  $\omega[N]$  is the scaled variance of  $N$ . A similar expression follows from Eq. (3.7) for the scaled variance  $\omega[B]$ . The scaled variances  $\omega[A]$  and  $\omega[B]$  depend on the fluctuations of the particle number via  $\omega[N]$ . Therefore,  $\omega[A]$  and  $\omega[B]$  are not strongly intensive quantities.

From Eqs. (3.6-3.8) one obtains expressions for  $\Delta[A, B]$  and  $\Sigma[A, B]$ , namely:

$$\Delta[A, B] = \frac{\langle N \rangle}{C_\Delta} \left[ \overline{\beta} \omega[\alpha] - \overline{\alpha} \omega[\beta] \right], \quad (3.10)$$

$$\Sigma[A, B] = \frac{\langle N \rangle}{C_\Sigma} \left[ \overline{\beta} \omega[\alpha] + \overline{\alpha} \omega[\beta] - 2 \left( \overline{\alpha\beta} - \overline{\alpha} \cdot \overline{\beta} \right) \right]. \quad (3.11)$$

Thus, the requirement that

$$\Delta[A, B] = \Sigma[A, B] = 1, \quad (3.12)$$

within the IPM leads to:

$$C_\Delta = \langle N \rangle \left[ \overline{\beta} \omega[\alpha] - \overline{\alpha} \omega[\beta] \right], \quad (3.13)$$

$$C_\Sigma = \langle N \rangle \left[ \overline{\beta} \omega[\alpha] + \overline{\alpha} \omega[\beta] - 2 \left( \overline{\alpha\beta} - \overline{\alpha} \cdot \overline{\beta} \right) \right]. \quad (3.14)$$

In the IPM the  $A$  and  $B$  quantities are expressed in terms of sums of the single particle variables,  $\alpha$  and  $\beta$ . Thus in order to calculate the normalization  $C_\Delta$  and  $C_\Sigma$  factors one has to measure the single particle quantities  $\alpha$  and  $\beta$ . However, this may not always be possible within a given experimental set-up. For example,  $A$  and  $B$  may be energies of particles measured by two calorimeters. Then one can study fluctuations in terms of  $\Delta[A, B]$  and  $\Sigma[A, B]$  but can not calculate the normalization factors which are proposed above.

We consider now two examples of specific pairs of extensive variables  $A$  and  $B$ . In the first example, we use the transverse momentum  $P_T = p_t^{(1)} + \dots + p_t^{(N)}$ , where  $p_t^{(i)}$  is the absolute value of the  $i^{\text{th}}$  particle transverse momentum, and the number of particles  $N$ . The requirement that

$$\Delta[P_T, N] = \Sigma[P_T, N] = 1 \quad (3.15)$$

for the IPM leads then to the normalization factors [43]

$$C_\Delta = C_\Sigma = \omega[p_t] \cdot \langle N \rangle, \quad \omega[p_t] \equiv \frac{\overline{p_t^2} - \overline{p_t}^2}{\overline{p_t}}, \quad (3.16)$$

where  $\omega[p_t]$  describes the single particle  $p_t$ -fluctuations.

As the second example let us consider the multiplicity fluctuations. Here  $A$  and  $B$  will denote the multiplicities of hadrons of types  $A$  and  $B$ , respectively (e.g., kaons and pions). One obtains [43]

$$C_\Delta = \langle B \rangle - \langle A \rangle, \quad C_\Sigma = \langle A \rangle + \langle B \rangle. \quad (3.17)$$

The normalization factors (3.16) and (3.17) are suggested to be used for the calculation for  $\Delta$  and  $\Sigma$  both in theoretical models and for the analysis of experimental data (see Ref. [43] for further details of the normalization procedure).

The  $\Phi$  measure, introduced some time ago [44], belongs to the  $\Sigma$  family within the current classification scheme. The fluctuation measure  $\Phi$  was introduced for the study of transverse momentum fluctuations. In the general case, when  $A = X$  represents any motional variable and  $B = N$  is the particle multiplicity, one gets:

$$\Phi_X = [\bar{x} \omega[x]]^{1/2} [\sqrt{\Sigma[X, N]} - 1]. \quad (3.18)$$

For the multiplicity fluctuations of hadrons belonging to non-overlapping types  $A$  and  $B$  the connection between the  $\Phi[A, B]$  and  $\Sigma[A, B]$  measures reads:

$$\Phi[A, B] = \frac{\sqrt{\langle A \rangle \langle B \rangle}}{\langle A \rangle + \langle B \rangle} [\sqrt{\Sigma[A, B]} - 1]. \quad (3.19)$$

The IPM plays an important role as the *reference model*. The deviations of real data from the IPM results Eq. (3.15) can be used to learn about the physical properties of the system. This resembles the situation in studies of particle multiplicity fluctuations. In this case, one uses the Poisson distribution  $P(N) = \exp(-\overline{N}) \overline{N}^N / N!$  with  $\omega[N] = 1$  as the reference model. The other reference value  $\omega[N] = 0$  corresponds to  $N = \text{const}$ , i.e., the absence of  $N$ -fluctuations. Values of  $\omega[N] > 1$  (or  $\omega[N] \gg 1$ ) correspond to “large” (or “very large”) fluctuations of  $N$ , and  $\omega[N] < 1$  (or  $\omega[N] \ll 1$ ) to “small” (or “very small”) fluctuations.

The fluctuation measures  $\Delta$  and  $\Sigma$  do not depend on the average size of the system and its fluctuations in several different model approaches, namely, statistical mechanics within the GCE, model of Multiple Independent Sources, Mixed Event Model (see Ref. [43] for details). Thus, one may expect that  $\Delta$  and  $\Sigma$  preserve their strongly intensive properties in many real experiments too. An extension of the strongly intensive fluctuation measures for higher order cumulants were suggested in recent paper [45].

### 3.2 $\Delta$ and $\Sigma$ Evaluated in Specific Models

The UrQMD [46] calculations of  $\Delta$  and  $\Sigma$  measures were performed in Refs. [47, 48]. The Monte Carlo simulations and analytical model results for  $\Delta[P_T, N]$  and  $\Sigma[P_T, N]$  were presented

in Ref. [49]. These measures were also studied in Ref. [50] for the ideal Bose and Fermi gases within the GCE. The GCE for the Boltzmann approximation satisfies the conditions of the IPM, i.e., Eq. (3.12) is valid. The following general relations were found [50]:

$$\Delta^{\text{Bose}}[P_T, N] < \Delta^{\text{Boltz}} = 1 < \Delta^{\text{Fermi}}[P_T, N] , \quad (3.20)$$

$$\Sigma^{\text{Fermi}}[P_T, N] < \Sigma^{\text{Boltz}} = 1 < \Sigma^{\text{Bose}}[P_T, N] , \quad (3.21)$$

i.e., the Bose statistics makes  $\Delta[P_T, N]$  smaller and  $\Sigma[P_T, N]$  larger than unity, whereas the Fermi statistics works in the opposite way. The Bose statistics of pions appears to be the main source of quantum statistics effects in a hadron gas with a temperature typical for the hadron system created in A+A collisions. It gives about 20% decrease of  $\Delta[P_T, N]$  and 10% increase of  $\Sigma[P_T, N]$ , at  $T \cong 150$  MeV with respect to the IPM results (3.12). The Fermi statistics of protons modifies insignificantly  $\Delta[P_T, N]$  and  $\Sigma[P_T, N]$  for typical values of  $T$  and  $\mu_B$ . Note that UrQMD takes into account several sources of fluctuations and correlations, e.g., the exact conservation laws and resonance decays. On the other hand, it does not include the effects of Bose and Fermi statistics. First experimental results on  $\Delta[P_T, N]$  and  $\Sigma[P_T, N]$  in p+p and Pb+Pb collisions have been reported in Refs. [51, 52, 53].

Now we consider the  $\Delta$  and  $\Sigma$  measures for two particle multiplicities  $N_1$  and  $N_2$ . Resonance decays, when particle species 1 and 2 appear simultaneously among the decay products, lead to the (positive) correlations between  $N_1$  and  $N_2$  numbers. Let  $N_1 = \pi^+$  and  $N_2 = \pi^-$  are the multiplicities of positively and negatively charged pions, respectively. A presence of two components is assumed: the correlated pion pairs coming from decays,  $R_{\pi\pi} \rightarrow \pi^+ + \pi^-$ , and the uncorrelated  $\pi^+$  and  $\pi^-$  from other sources. The  $\pi^+$  and  $\pi^-$  numbers are then equal to:

$$\pi^+ = n_+ + R_{\pi\pi} , \quad \pi^- = n_- + R_{\pi\pi} , \quad (3.22)$$

where  $R_{\pi\pi}$  is the number of resonances decaying into  $\pi^+\pi^-$  pairs, while  $n_+$  and  $n_-$  are the numbers of uncorrelated  $\pi^+$  and  $\pi^-$ , respectively.

Using approximate relations,

$$\omega[\pi^+] \cong \omega[\pi^-] \cong \omega[R_{\pi\pi}] \cong 1 , \quad (3.23)$$

one obtains two alternative expressions for the number of  $R_{\pi\pi}$ -resonances [54]:

$$\frac{\langle R_{\pi\pi} \rangle}{\langle \pi^- \rangle + \langle \pi^+ \rangle} \cong \frac{\langle \pi^+ \pi^- \rangle - \langle \pi^+ \rangle \langle \pi^- \rangle}{\langle \pi^+ \rangle + \langle \pi^- \rangle} \equiv \rho[\pi^+, \pi^-] , \quad (3.24)$$

$$\frac{\langle R_{\pi\pi} \rangle}{\langle \pi^- \rangle + \langle \pi^+ \rangle} \cong \frac{1 - \Sigma[\pi^+, \pi^-]}{2} , \quad (3.25)$$

i.e.,  $R_{\pi\pi}$  can be calculated using the measurable quantities of e-by-e fluctuations. As a result, these resonance abundances, which are difficult to be measured by other methods, can be estimated by measuring the fluctuations and correlations of the numbers of stable hadrons. Note that an idea to use the e-by-e fluctuations of particle number ratios to estimate the number of hadronic resonances was suggested for the first time in Ref. [55].

The analysis of  $\pi^+$  and  $\pi^-$  fluctuations and correlations from resonance decays is done in Ref. [54]. It is based on the HRG model, both in the GCE and CE, and on the relativistic transport

model UrQMD. This analysis illustrates a role of the centrality selection, limited acceptance, and global charge conservation in A+A collisions. We present now the results for Eq. (3.24) and (3.25) in Pb+Pb and p+p collisions. Note that  $\rho$  in Eq. (3.24) is an intensive but not strongly intensive quantity. Thus, it is expected to be sensitive to the system size fluctuations. On the other hand, the  $\Sigma$  in Eq. (3.25) is the strongly intensive measure and it should keep the same value in a presence of the system size fluctuations.

The samples of 5% central Pb+Pb collision events at  $\sqrt{s_{NN}} = 6.27$  and 17.3 GeV are considered. These UrQMD results are compared with those for most central Pb+Pb collisions at zero impact parameter,  $b = 0$  fm, and for  $p + p$  reactions at the same collision energies. Several mid-rapidity windows  $-\Delta y/2 < y < \Delta y/2$  for final  $\pi^+$  and  $\pi^-$  particles are considered.

A width of the rapidity window  $\Delta y$  is an important parameter. The two hadrons which are the products of a resonance decay have, in average, a rapidity difference of the order of unity. Therefore, while searching for the effects of resonance decays one should choose  $\Delta y \geq 1$  to enlarge a probability for simultaneous hit into the rapidity window  $\Delta y$  of both correlated hadrons (e.g.,  $\pi^+$  and  $\pi^-$ ) from resonance decays. Thus,  $\Delta y$  should be *large* enough. However,  $\Delta y$  should be *small* in comparison to the whole rapidity interval  $\Delta Y \approx \ln(\sqrt{s_{NN}}/m)$  accessible for final hadron with mass  $m$ . Only for  $\Delta y \ll \Delta Y$  one can expect a validity of the GCE results. Considering a small part of the statistical system, one does not need to impose the restrictions of the exact global charge conservations: the GCE which only regulates the average values of the conserved charges is fully acceptable. For large  $\Delta y$ , when the detected hadrons correspond to an essential part of the whole system, the effects of the global charge conservation become more important. In the HRG this should be treated within the CE, where the conserved charges are fixed for all microscopic states. The global charge conservation influences the particle number fluctuations and introduces additional correlations between numbers of different particle species.

The UrQMD values of correlation parameter  $\rho[\pi^+, \pi^-]$  in 5% central Pb+Pb collision events are shown by full circles in Fig. 5(a) and full boxes in 5(b) as functions of the acceptance windows  $\Delta y$ . The UrQMD results for the most central Pb+Pb collision events with zero impact parameter,  $b = 0$  fm, are shown by open symbols. The triangles show the results of the UrQMD simulations in  $p + p$  reactions. The collision energy is taken as  $\sqrt{s_{NN}} = 6.27$  GeV in Fig. 5(a) and  $\sqrt{s_{NN}} = 17.3$  GeV in Fig. 5(b). The windows at the center of mass mid-rapidity are taken as  $\Delta y = 0.2, 1, 2, 3, 4$ , and  $\infty$ . A symbol  $\infty$  denotes the case when all final state particles are detected (i.e., a full  $4\pi$ -acceptance). Note that the UrQMD model does not assume any, even local, thermal and/or chemical equilibration. Therefore, a connection between the UrQMD and HRG results for particle number fluctuations and correlations is a priori unknown.

For the 5% most central Pb+Pb collisions the correlation  $\rho[\pi^+, \pi^-]$  increases with  $\Delta y$ . As seen from Fig. 5(b), this increase is rather strong at high collision energy: at large  $\Delta y$ , the value of  $\rho[\pi^+, \pi^-]$  becomes much larger than the HGM results in both the CE and GCE. The behavior of  $\omega[\pi^+]$  and  $\omega[\pi^-]$  is rather similar to that of  $\rho[\pi^+, \pi^-]$ .

Selecting within the UrQMD simulations the most central Pb+Pb collision events with zero impact parameter  $b = 0$  fm, one finds essentially smaller values of  $\rho[\pi^+, \pi^-]$  (open symbols in Fig. 5). This means that in the 5% centrality bin of Pb+Pb collision events large fluctuations of the number of nucleon participants (i.e., the volume fluctuations) are present. These volume fluctuations produce large additional contributions to the scaled variances of pions and to the correlation

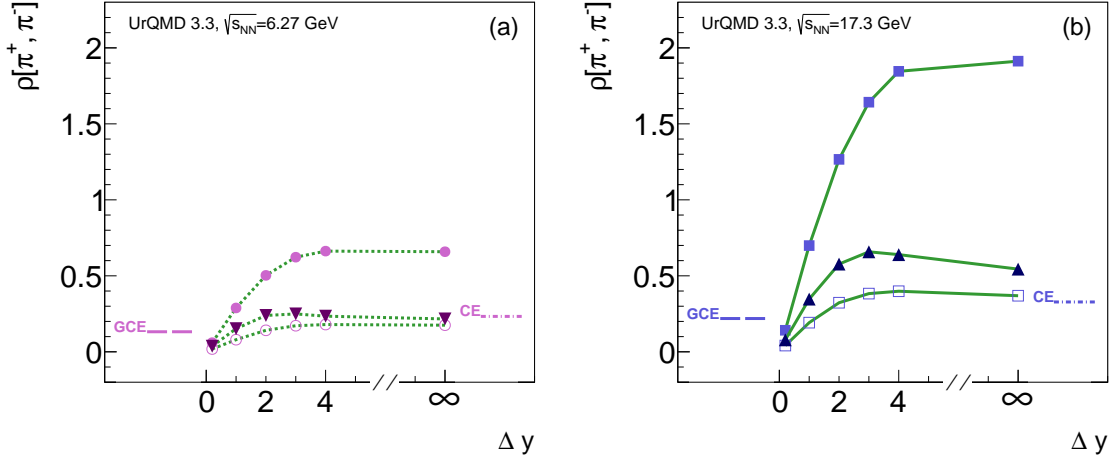


**Figure 5:** The UrQMD results for  $\rho[\pi^+, \pi^-]$  in central Pb+Pb and inelastic  $p + p$  collisions for the mid-rapidity windows  $\Delta y$ , i.e., the center of mass rapidities  $y$  of final  $\pi^+$  and  $\pi^-$  satisfy the condition  $-\Delta Y < y < \Delta Y$ . Full circles and squares correspond to the 5% centrality selection and the open ones to the most central Pb+Pb collision events with zero impact parameter  $b = 0$  fm. Triangles correspond to the UrQMD simulations of inelastic  $p + p$  interactions. The collision energies are:  $\sqrt{s_{NN}} = 6.27$  GeV in (a) and  $\sqrt{s_{NN}} = 17.3$  GeV in (b). The horizontal dashed and dashed-dotted lines show, respectively, the GCE and CE results taken at the corresponding  $\sqrt{s_{NN}}$ .

parameter  $\rho[\pi^+, \pi^-]$ . They become more and more important with increasing collision energy. This is due to an increase of the number of pions per participating nucleon with increasing collision energy. However, one hopes that these volume fluctuations will be canceled out to a large extent when they are combined in the strongly intensive measures. Note also that the UrQMD results for  $\rho[\pi^+, \pi^-]$  in inelastic  $p + p$  collisions, shown in Fig. 5 by triangles, are qualitatively similar to those in Pb+Pb collisions at  $b = 0$  fm.

The UrQMD results for  $\Sigma[\pi^+, \pi^-]$  in Pb+Pb collisions at  $\sqrt{s_{NN}} = 6.27$  GeV and 17.3 GeV are presented in Fig. 6(a) and (b), respectively, as a function of the acceptance window  $\Delta y$  at mid-rapidity. In contrast to the results shown in Fig. 5, both centrality selections in Pb+Pb collisions (5% centrality bin and  $b = 0$  fm) lead to very similar results for  $\Sigma[\pi^+, \pi^-]$  shown in Fig. 6. This means that the measure  $\Sigma[\pi^+, \pi^-]$  has the strongly intensive properties, at least in the UrQMD simulations. The UrQMD results in  $p + p$  reactions are close to those in Pb+Pb ones.

The GCE and CE results of the HRG are presented in Figs. 5 and 6 by the horizontal dashed and dashed-dotted lines, respectively. The UrQMD results for  $\Sigma[\pi^+, \pi^-]$ , presented in Fig. 6, demonstrate a strong dependence on the size of rapidity window  $\Delta y$ . At  $\Delta y = 1$  these results are close to those of the GCE HRM. On the other hand, with increasing  $\Delta y$  the role of exact charge conservation becomes more and more important. From Fig. 6, one observes that the UrQMD values of  $\Sigma[\pi^+, \pi^-]$  at large  $\Delta y$  are close to the CE results.

As seen from Fig. 5, a similar correspondence between the UrQMD results for  $\rho[\pi^+, \pi^-]$  in Pb+Pb collisions at  $b = 0$  fm and their GCE and CE values is approximately valid. However, this is not the case for the 5% most central Pb+Pb events. In that centrality bin the volume fluctuations

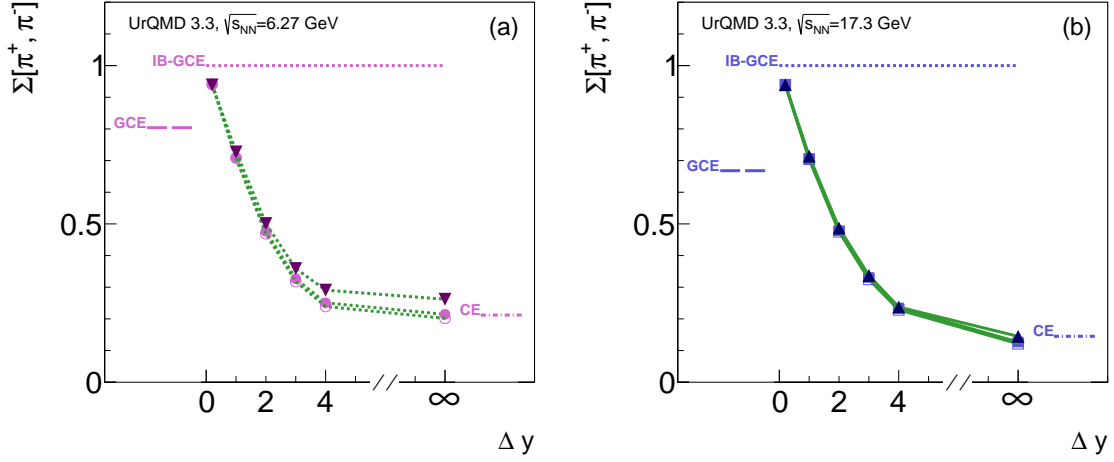


**Figure 6:** The same as in Fig. 5 but for  $\Sigma[\pi^+, \pi^-]$ .

give the dominant contributions to  $\rho[\pi^+, \pi^-]$  for large  $\Delta y$ .

For very small acceptance,  $\Delta y \ll 1$ , one expects an approximate validity of the Poisson distribution for any type of the detected particles. Their scaled variances are then close to unity, i.e.,  $\omega[\pi^-] \cong \omega[\pi^+] \cong 1$ . Particle number correlations, due to both the resonance decays and the global charge conservation, become negligible, i.e.,  $\rho[\pi^+, \pi^-] \ll 1$ . These expectations are indeed supported by the UrQMD results at  $\Delta y = 0.2$  presented in Fig. 5. Therefore, one expects  $\Sigma[\pi^+, \pi^-] \rightarrow 1$  at  $\Delta y \rightarrow 0$ . This expectation is also valid, as seen from the UrQMD results at  $\Delta y = 0.2$  presented in Fig. 6.

#### 4. Incomplete Particle Identification

Fluctuations of the chemical (particle-type) composition of hadronic final states in A+A collisions are expected to be sensitive to the phase transition between hadronic and partonic matter. First experimental results on e-by-e chemical fluctuations have already been published from the CERN SPS and BNL RHIC, and more systematic measurements are in progress.

Studies of chemical fluctuations in general require to determine the number of particles of different hadron species (e.g., pions, kaons, and protons) e-by-e. A serious experimental problem in such measurements is incomplete particle identification, i.e., the impossibility to identify uniquely the type of each detected particle. The effect of particle misidentification distorts the measured fluctuation quantities. For this reason the analysis of chemical fluctuations is usually performed in a small acceptance, where particle identification is relatively reliable. However, an important part of the information on e-by-e fluctuations in full phase space is then lost.

Although it is usually impossible to identify each detected particle, one can nevertheless determine with high accuracy the average multiplicities (averaged over many events) for different hadron species.



#### 4.1 The Identity Method

The identity variable was introduced in Ref. [56], and in Ref. [57] a new experimental technique called the *identity method* was proposed. It solved the misidentification problem for one specific combination of the second moments in a system of two hadron species ('kaons' and 'pions'). In Refs. [58, 59] this method was extended to show that all the second moments as well as the higher moments of the joint multiplicity distribution of particles of different types can be uniquely reconstructed in spite of the effects of incomplete identification. Notably, the results [58, 59] can be used for an arbitrary number  $k \geq 2$  of hadron species. It is assumed that particle identification is achieved by measuring the particle mass  $m$ . Since any measurement is of finite resolution, we deal with continuous distributions of observed masses denoted as  $\rho_j(m)$  and normalized as ( $j = 1, \dots, k \geq 2$ )

$$\int dm \rho_j(m) = \langle N_j \rangle. \quad (4.1)$$

Note that for experimental data the functions  $\rho_j(m)$  for particles of type  $j$  are obtained from the inclusive distribution of the  $m$ -values for all particles from all collision events. The identity variables  $w_j(m)$  are defined as

$$w_j(m) \equiv \frac{\rho_j(m)}{\rho(m)}, \quad \rho(m) \equiv \sum_{i=1}^k \rho_i(m). \quad (4.2)$$

Complete identification (CI) of particles corresponds to distributions  $\rho_j(m)$  which do not overlap. In this case,  $w_j = 0$  for all particle species  $i \neq j$  and  $w_j = 1$  for the  $j$ th species. When the distributions  $\rho_j(m)$  overlap,  $w_j(m)$  can take the value of any real number from  $[0, 1]$ . We introduce the quantities

$$W_j \equiv \sum_{i=1}^{N(n)} w_j(m_i), \quad W_j^2 \equiv \left( \sum_{i=1}^{N(n)} w_j(m_i) \right)^2, \quad W_p W_q \equiv \left( \sum_{i=1}^{N(n)} w_p(m_i) \right) \times \left( \sum_{i=1}^{N(n)} w_q(m_i) \right), \quad (4.3)$$

with  $j = 1, \dots, k$  and  $1 \leq p < q \leq k$ , and define their event averages as

$$\langle W_j^2 \rangle = \frac{1}{N_{\text{ev}}} \sum_{n=1}^{N_{\text{ev}}} W_j^2, \quad \langle W_p W_q \rangle = \frac{1}{N_{\text{ev}}} \sum_{n=1}^{N_{\text{ev}}} W_p W_q, \quad (4.4)$$

where  $N_{\text{ev}}$  is the number of events, and  $N(n) = N_1(n) + \dots + N_k(n)$  is the total multiplicity in the  $n$ th event. Each experimental event is characterized by a set of particle masses  $\{m_1, m_2, \dots, m_N\}$ , for which one can calculate the full set of identity variables:  $\{w_j(m_1), w_j(m_2), \dots, w_j(m_N)\}$ , with  $j = 1, \dots, k$ . Thus, the quantities  $W_j$ ,  $W_j^2$ , and  $W_p W_q$  are completely defined for each event, and their average values (4.4) can be found experimentally by straightforward e-by-e averaging. The main idea is to find the relations between these  $W$ -quantities and the unknown moments of the multiplicity distribution  $\langle N_j^2 \rangle$  and  $\langle N_p N_q \rangle$ . In the case of CI, one finds  $W_j = N_j$ , thus, Eq. (4.4) yields

$$\langle W_j^2 \rangle = \langle N_j^2 \rangle, \quad \langle W_p W_q \rangle = \langle N_p N_q \rangle. \quad (4.5)$$

## 4.2 Second Moments of Chemical Fluctuations

The quantities  $\langle W_j^2 \rangle$  and  $\langle W_p W_q \rangle$  can be calculated as follows [58]

$$\langle W_j^2 \rangle = \sum_{i=1}^k \langle N_i \rangle [u_{ji}^2 - (u_{ji})^2] + \sum_{i=1}^k \langle N_i^2 \rangle (u_{ji})^2 + 2 \sum_{1 \leq i < l \leq k} \langle N_i N_l \rangle u_{ji} u_{jl} , \quad (4.6)$$

$$\langle W_p W_q \rangle = \sum_{i=1}^k \langle N_i \rangle [u_{pqi} - u_{pi} u_{qi}] + \sum_{i=1}^k \langle N_i^2 \rangle u_{pi} u_{qi} + \sum_{1 \leq i < l \leq k} \langle N_i N_l \rangle [u_{pi} u_{ql} + u_{pl} u_{qi}] . \quad (4.7)$$

In Eqs. (4.6) and (4.7),  $\mathcal{P}(N_1, \dots, N_k)$  is the multiplicity distribution,  $P_i(m) \equiv \rho_i(m) / \langle N_i \rangle$  are the mass probability distributions of the  $i$ th species, and ( $s = 1, 2$ )

$$u_{ji}^s \equiv \frac{1}{\langle N_i \rangle} \int dm w_j^s(m) \rho_i(m) , \quad u_{pqi} \equiv \frac{1}{\langle N_i \rangle} \int dm w_p(m) w_q(m) \rho_i(m) . \quad (4.8)$$

In the case of CI, when the distributions  $\rho_j(m)$  do not overlap, one finds that

$$u_{ji}^s = \delta_{ji} , \quad u_{pqi} = 0 , \quad (4.9)$$

and Eqs. (4.6) and (4.7) reduce then to Eq. (4.5). The incomplete particle identification transforms the second moments  $\langle N_j^2 \rangle$  and  $\langle N_p N_q \rangle$  to the quantities  $\langle W_j^2 \rangle$  and  $\langle W_p W_q \rangle$ , respectively. Each of the later quantities contains linear combinations of all the first and second moments,  $\langle N_i \rangle$  and  $\langle N_i^2 \rangle$ , as well as all the correlation terms  $\langle N_i N_l \rangle$ . Having introduced the notations

$$\langle W_j^2 \rangle - \sum_{i=1}^k \langle N_i \rangle [u_{ji}^2 - (u_{ji})^2] \equiv b_j , \quad \langle W_p W_q \rangle - \sum_{i=1}^k \langle N_i \rangle [u_{pqi} - u_{pi} u_{qi}] \equiv b_{pq} , \quad (4.10)$$

one can transform Eqs. (4.6) and (4.7) to the following form:

$$\sum_{i=1}^k \langle N_i^2 \rangle u_{ji}^2 + 2 \sum_{1 \leq i < l \leq k} \langle N_i N_l \rangle u_{ji} u_{jl} = b_j , \quad j = 1, 2, \dots, k , \quad (4.11)$$

$$\sum_{i=1}^k \langle N_i^2 \rangle u_{pi} u_{qi} + \sum_{1 \leq i < l \leq k} \langle N_i N_l \rangle (u_{pi} u_{ql} + u_{pl} u_{qi}) = b_{pq} , \quad 1 \leq p < q \leq k . \quad (4.12)$$

The right-hand side of Eqs. (4.11) and (4.12) defined by Eq. (4.10) are experimentally measurable quantities. The same is true for the coefficients  $u_{ji}^s$  (with  $s = 1$  and 2) entering the left-hand side of Eqs. (4.11) and (4.12). Therefore, Eqs. (4.11) and (4.12) represent a system of  $k + k(k-1)/2$  linear equations for the  $k$  second moments  $\langle N_j^2 \rangle$  with  $j = 1, \dots, k$  and  $k(k-1)/2$  correlators  $\langle N_p N_q \rangle$  with  $1 \leq p < q \leq k$ . In order to solve Eqs. (4.11) and (4.12) we introduce the  $[k + k(k-1)/2] \times [k + k(k-1)/2]$  matrix  $A$

$$A = \left( \begin{array}{ccc|ccc} a_1^1 & \dots & a_1^k & a_1^{12} & \dots & a_1^{(k-1)k} \\ \cdot & \cdot & \cdot & \cdot & \cdot & \cdot \\ \cdot & \cdot & \cdot & \cdot & \cdot & \cdot \\ a_k^1 & \dots & a_k^k & a_k^{12} & \dots & a_k^{(k-1)k} \\ \hline a_{12}^1 & \dots & a_{12}^k & a_{12}^{12} & \dots & a_{12}^{(k-1)k} \\ \cdot & \cdot & \cdot & \cdot & \cdot & \cdot \\ \cdot & \cdot & \cdot & \cdot & \cdot & \cdot \\ a_{(k-1)k}^1 & \dots & a_{(k-1)k}^k & a_{(k-1)k}^{12} & \dots & a_{(k-1)k}^{(k-1)k} \end{array} \right) , \quad (4.13)$$

where

$$a_j^i \equiv u_{ji}^2, \quad 1 \leq i, j \leq k; \quad a_i^{pq} \equiv 2u_{ip}u_{iq}, \quad 1 \leq p < q \leq k, \quad i = 1, \dots, k; \quad (4.14)$$

$$a_{pq}^i \equiv u_{pi}u_{qi}, \quad 1 \leq p < q \leq k, \quad i = 1, \dots, k; \quad (4.15)$$

$$a_{pq}^{lm} \equiv u_{pl}u_{qm} + u_{ql}u_{pm}, \quad 1 \leq p < q \leq k, \quad 1 \leq l < m \leq k. \quad (4.16)$$

The solution of Eqs. (4.11) and (4.12) can be presented by Cramer's formulas in terms of the determinants

$$\langle N_j^2 \rangle = \frac{\det A_j}{\det A}, \quad \langle N_p N_q \rangle = \frac{\det A_{pq}}{\det A}, \quad (4.17)$$

where the matrices  $A_j$  and  $A_{pq}$  are obtained by substituting in the matrix  $A$  the column  $a_1^j, \dots, a_k^j, a_{12}^j, \dots, a_{(k-1)k}^j$  and the column  $a_1^{pq}, \dots, a_k^{pq}, a_{12}^{pq}, \dots, a_{(k-1)k}^{pq}$ , respectively, for the column  $b_1, \dots, b_k, b_{12}, \dots, b_{(k-1)k}$ . Therefore, if  $\det A \neq 0$ , the system of linear equations (4.11) and (4.12) has a unique solution (4.17) for all the second moments. In the case of CI (4.9), one finds  $\det A = 1$ ,  $\det A_j = b_j$ , and  $\det A_{pq} = b_{pq}$ . The solution (4.17) reduces then to Eq. (4.5).

Introducing the  $[k + k(k-1)/2]$ -vectors

$$\mathcal{N} \equiv \begin{pmatrix} \langle N_1^2 \rangle \\ \dots \\ \langle N_k^2 \rangle \\ \langle N_1 N_2 \rangle \\ \dots \\ \langle N_{k-1} N_k \rangle \end{pmatrix}, \quad \mathcal{B} \equiv \begin{pmatrix} b_1 \\ \dots \\ b_k \\ b_{12} \\ \dots \\ b_{(k-1)k} \end{pmatrix}, \quad (4.18)$$

one can write Eqs. (4.11) and (4.12) in the matrix form  $A\mathcal{N} = \mathcal{B}$ . The solution (4.17) can be then rewritten as

$$\mathcal{N} = A^{-1} \mathcal{B}, \quad (4.19)$$

where  $A^{-1}$  is the inverse matrix of  $A$ . For two particle species,  $k = 2$ , this solution takes the form

$$\begin{pmatrix} \langle N_1^2 \rangle \\ \langle N_2^2 \rangle \\ \langle N_1 N_2 \rangle \end{pmatrix} = \begin{pmatrix} u_{11}^2 & u_{12}^2 & 2u_{11}u_{12} \\ u_{21}^2 & u_{22}^2 & 2u_{21}u_{22} \\ u_{11}u_{21} & u_{12}u_{22} & u_{11}u_{22} + u_{12}u_{21} \end{pmatrix}^{-1} \begin{pmatrix} b_1 \\ b_2 \\ b_{12} \end{pmatrix}. \quad (4.20)$$

Then Eq. (4.20) yields

$$\langle N_1^2 \rangle = \frac{b_1 u_{22}^2 + b_2 u_{12}^2 - 2b_{12} u_{12} u_{22}}{(u_{11} u_{22} - u_{12} u_{21})^2}, \quad (4.21)$$

$$\langle N_2^2 \rangle = \frac{b_2 u_{11}^2 + b_1 u_{21}^2 - 2b_{12} u_{21} u_{11}}{(u_{11} u_{22} - u_{12} u_{21})^2}, \quad (4.22)$$

$$\langle N_1 N_2 \rangle = \frac{b_{12} (u_{11} u_{22} + u_{12} u_{21}) - b_1 u_{22} u_{21} - b_2 u_{11} u_{12}}{(u_{11} u_{22} - u_{12} u_{21})^2}. \quad (4.23)$$

The above procedure eliminates the effect of misidentification and provides the values of all the second moments  $\langle N_j^2 \rangle$  and  $\langle N_p N_q \rangle$  in a model-independent way, as they would be obtained in an experiment in which each particle is uniquely identified. This method was generalized to determine third and higher moments of the multiplicity distributions in events consisting of an arbitrary number of different particle species in Ref. [59]. Measurements of the third and higher moments of e-by-e fluctuations are expected to be more sensitive for the search of the CP in A+A collisions [60, 61]. First results on fluctuations based on the identity method were presented in Refs. [52, 62, 63].

## 5. Fluctuations at the Critical Point

In this section we consider the van der Waals (VDW) equation of state with both repulsive ( $b > 0$ ) and attractive ( $a > 0$ ) terms (see, e.g., Refs. [64, 65]):

$$p(V, T, N) = \frac{NT}{V - bN} - a \frac{N^2}{V^2} = \frac{nT}{1 - bn} - an^2. \quad (5.1)$$

It gives an example of a system with the CP. The equation of state (5.1) was suggested in 1873, and for his work van der Waals obtained the Nobel Prize in physics in 1910. The particle proper volume parameter in Eq. (5.1) equals to  $b = 4 \cdot (4\pi r^3/3)$  with  $r$  being the corresponding hard sphere radius of particle. The  $b$  parameter describes the repulsion between particles and can be rigorously obtained (in particular, a factor of 4 in the expression for  $b$ ) for a gas of the hard balls at low density (see, e.g., Ref. [65]).

### 5.1 Phase Diagram

The VDW equation of state contains a 1<sup>st</sup> order liquid-gas phase transition and CP. The thermodynamical quantities at the CP are equal to [65]:

$$T_c = \frac{8a}{27b}, \quad n_c = \frac{1}{3b}, \quad p_c = \frac{a}{27b^2}. \quad (5.2)$$

The VDW equation (5.1) can be then rewritten in the following dimensionless (reduced) form:

$$\tilde{p} = \frac{8\tilde{T}\tilde{n}}{3 - \tilde{n}} - 3\tilde{n}^2, \quad (5.3)$$

where  $\tilde{n} = n/n_c$ ,  $\tilde{p} = p/p_c$ , and  $\tilde{T} = T/T_c$ . In the dimensionless presentation (5.3) the VDW equation has a universal form independent of the values of  $a$  and  $b$ , and the CP (5.2) is transformed to  $\tilde{T}_c = \tilde{p}_c = \tilde{n}_c = 1$ .

The dimensionless VDW isotherms are presented in Fig. 7 (*left*) as functions of  $\tilde{v} \equiv \tilde{n}^{-1}$ . To describe the phase coexistence region below the critical temperature the VDW isotherms should be corrected by the well known Maxwell construction of *equal areas*. These corrected parts of the VDW isotherms are shown by the solid horizontal lines. Figure 7 (*right*) depicts the liquid-gas coexistence region on the  $(\tilde{n}, \tilde{T})$  plane.

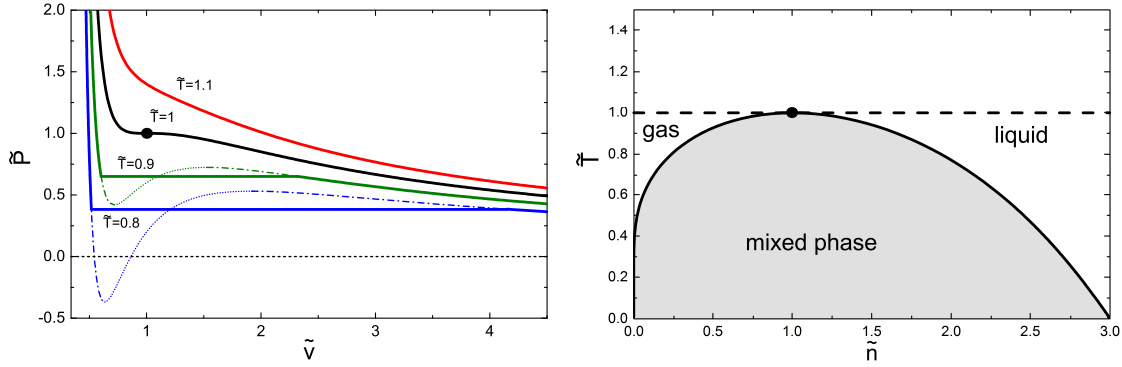


**Figure 7:** *Left:* The dimensionless form of the VDW isotherms for pressure,  $\tilde{p}$ , versus the volume per particle  $\tilde{v} = \tilde{n}^{-1}$ . The dashed-dotted lines present the metastable parts of the VDW isotherms at  $\tilde{T} < 1$ , whereas the dotted lines correspond to unstable parts. The full circle on the  $\tilde{T} = 1$  isotherm corresponds to the CP. *Right:* The phase diagram for the VDW equation of state on the  $(\tilde{n}, \tilde{T})$  plane. The phase coexistence region resulting from the Maxwell construction is depicted by grey shaded area.

## 5.2 The GCE Formulation and Particle Number Fluctuations

As the first step, the VDW equation (5.1) will be transformed to the GCE. The GCE formulation will be then used to calculate the particle number fluctuations in the VDW gas. These calculations were done in Ref. [66], where details can be found. The GCE form of the VDW equation of state has its simplest form for the particle number density,

$$n(T, \mu) = \frac{n_{\text{id}}(T, \mu^*)}{1 + b n_{\text{id}}(T, \mu^*)}, \quad \mu^* = \mu - b \frac{nT}{1 - bn} + 2an, \quad (5.4)$$

as a function of temperature  $T$  and chemical potential  $\mu$ . If  $a = b = 0$ , the function (5.4) is reduced to the ideal gas particle number density. Note that  $\mu$  regulates  $\langle N \rangle_{\text{gce}}$ , i.e.,  $N$  plays the role of conserved charge, and no antiparticles are introduced. For the ideal Boltzmann gas one obtains

$$n_{\text{id}}(T, \mu) = \exp\left(\frac{\mu}{T}\right) \frac{g m^2 T}{2\pi^2} K_2\left(\frac{m}{T}\right), \quad (5.5)$$

where  $g$  is the degeneracy factor,  $m$  is the particle mass, and  $K_2$  is the modified Hankel function. The function  $n(T, \mu)$  is the solution of transcendental equation (5.4). The GCE pressure  $p(T, \mu)$  for the VDW equation of state is obtained substituting  $n$  in Eq. (5.1) by function  $n(T, \mu)$  (5.4).

The variance of the total particle number in the GCE can be calculated as

$$\text{Var}[N] \equiv \langle N^2 \rangle - \langle N \rangle^2 = T \left( \frac{\partial \langle N \rangle}{\partial \mu} \right)_{T,V} = TV \left( \frac{\partial n}{\partial \mu} \right)_T, \quad (5.6)$$

where symbol  $\langle \dots \rangle$  denotes the GCE averaging, and  $n(T, \mu)$  is the particle number density in the GCE. The scaled variance for the particle number fluctuations is then [66]:

$$\omega[N] \equiv \frac{\text{Var}[N]}{\langle N \rangle} = \frac{T}{n} \left( \frac{\partial n}{\partial \mu} \right)_T = \left[ \frac{1}{(1 - bn)^2} - \frac{2an}{T} \right]^{-1}. \quad (5.7)$$

It is clearly seen from Eq. (5.7) that in the VDW gas the repulsive interactions suppress the particle number fluctuations, whereas the attractive interactions lead to their enhancement. Note that for

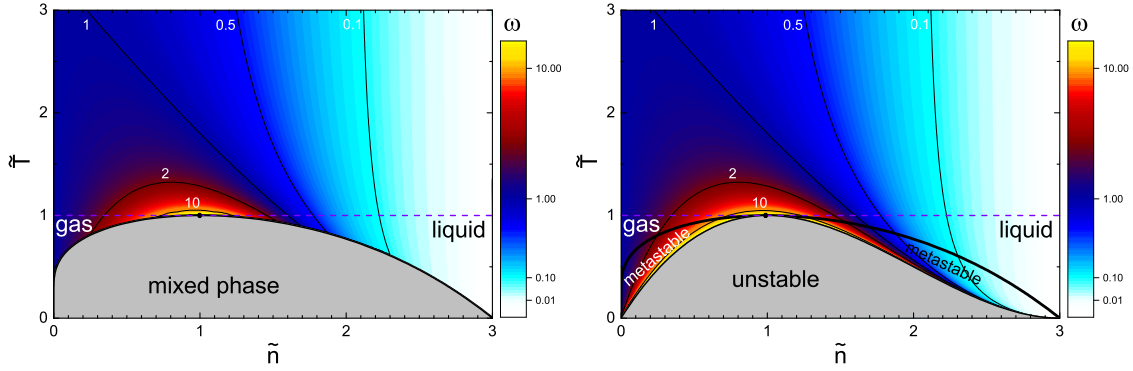


**Figure 8:** *Left:* The lines of constant values of the scaled variance  $\omega[N]$  are shown on the  $(\tilde{n}, \tilde{T})$  phase diagram, outside of the mixed phase region. *Right:* The lines of constant values of the scaled variance  $\omega[N]$  are shown on the  $(\tilde{n}, \tilde{T})$  phase diagram for both stable and metastable pure phases. The boundary between stable and metastable phases is depicted by the thick black line, and the unstable region is depicted by the gray area.

$a = 0$  the scaled variance (5.7) is reduced to the result for the excluded volume model obtained earlier in Ref. [67].

The scaled variance (5.7) expressed in terms  $\tilde{n}$  and  $\tilde{T}$  equals to

$$\omega[N] = \frac{1}{9} \left[ \frac{1}{(3 - \tilde{n})^2} - \frac{\tilde{n}}{4\tilde{T}} \right]^{-1}. \quad (5.8)$$

In Fig. 8 the lines of constant values of  $\omega[N]$  are shown on the  $(\tilde{n}, \tilde{T})$  phase diagram outside of the mixed phase region. At any fixed value of  $\tilde{T}$ , the particle number fluctuations (5.8) approach to those of the ideal gas, i.e.,  $\omega[N] \cong 1$ , at  $\tilde{n} \rightarrow 0$ , and become small,  $\omega[N] \ll 1$ , at  $\tilde{n} \rightarrow 3$ . As it should be, the scaled variance (5.8) is always positive for all possible values of  $\tilde{n}$  and  $\tilde{T}$  outside of the mixed phase region. At  $\tilde{T} \rightarrow 0$  this is insured by simultaneous limiting behavior of  $\tilde{n} \rightarrow 0$  in the pure gaseous phase and  $\tilde{n} \rightarrow 3$  in the pure liquid phase.

### 5.3 Critical Point

At the CP ( $\tilde{T} = \tilde{n} = 1$ ) the scaled variance of the particle number fluctuations diverges in the GCE. To study the behavior of  $\omega[N]$  in a vicinity of the critical point we introduce the quantities  $\tau = \tilde{T} - 1 \ll 1$  and  $\rho = \tilde{n} - 1 \ll 1$ . Expanding (5.8) at small  $\tau$  and  $\rho$  and keeping only the lowest orders of them one finds

$$\omega[N] \cong \frac{4}{9} \left[ \tau + \frac{3}{4}\rho^2 + \tau\rho \right]^{-1}. \quad (5.9)$$

In particular,

$$\omega[N] \cong \frac{4}{9} \tau^{-1} \text{ at } \rho = 0, \quad \text{and } \omega[N] \cong \frac{16}{27} \rho^{-2} \text{ at } \tau = 0. \quad (5.10)$$

Note that thermodynamical parameters  $\tilde{T}$  and  $\tilde{n}$  correspond to points outside the mixed phase region. This is shown in Fig. 8 *left*. Thus, in Eqs. (5.9) and (5.10), parameter  $\tau$  is positive, while  $\rho$  can be both positive and negative.

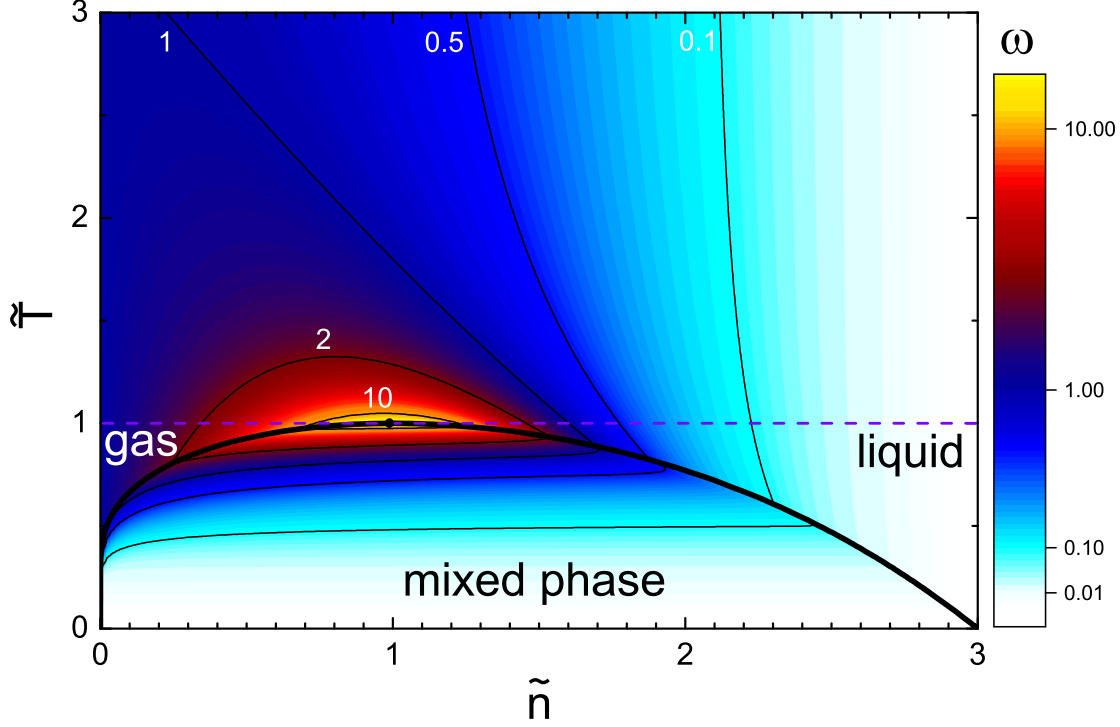


**Figure 9:** The lines of constant values of  $\omega[N]$  are shown on the phase diagram for  $0 < \tilde{T} < 3$  and for all possible  $\tilde{n}$  values, for stable states both inside and outside the mixed phase region.

The VDW equation of state permits the existence of metastable phases of super-heated liquid and super-cooled gas. These states are depicted by the dash-dotted lines on the VDW isotherms in Fig. 7 (*left*). In metastable phases the system is assumed to be uniform and, therefore, one can use Eq. (5.8) to calculate particle number fluctuations in these phases.

The lines of constant values of  $\omega[N]$  are shown on the  $(\tilde{n}, \tilde{T})$  phase diagram in Fig. 8 *right* for both stable and metastable pure phases, while the unstable region is depicted by the gray area. It is seen that the scaled variance remains finite, and diverges only at the boundary between the metastable and unstable regions. We recall that at this boundary  $\partial\tilde{p}/\partial\tilde{n} = 0$ , where  $\tilde{p}$  is the dimensionless CE pressure (5.3). One can easily show using Eqs. (5.3) and (5.8) that  $\omega[N] \rightarrow \infty$  when  $\partial\tilde{p}/\partial\tilde{n} = 0$ . Note that metastable regions of the equation of state can be reached within fast non-equilibrium processes, whereas the unstable region is physically forbidden. Note also that the thermodynamical relations are not fulfilled in the unstable region, e.g., nonphysical behavior with  $\omega[N] < 0$  is found in this region.

Finally, the scaled variance  $\omega[N]$  is shown in Fig. 9 for all possible values of  $\tilde{n}$  and  $\tilde{T}$ , both inside and outside of the mixed phase. Now only thermodynamically stable states are considered. Details of the calculations inside the mixed phase are presented in Ref. [66]. In a vicinity of the critical point inside the mixed phase we introduce  $0 < t = 1 - \tilde{T} \ll 1$  and find at  $t \rightarrow 0$ ,

$$\omega[N] \cong \frac{16}{9} t^{-1}. \quad (5.11)$$

Thus, the scaled variance  $\omega[N]$  diverges at the critical point reached from both outside and inside



the mixed phase.

## 6. Summary

1. The global conservation of energy and conserved charges influences the measured e-by-e fluctuations of all observables. Thus, to calculate these fluctuations within statistical mechanics one should properly choose the statistical ensemble. The GCE, CE, and MCE are only some particular examples. Real situation may correspond to very different externally given distributions of the volume  $V$ , energy  $E$ , and conserved charge(s)  $Q$ .

2. To avoid the trivial contributions from the system size fluctuations the strongly intensive measures of e-by-e fluctuations should be used. These  $\Delta[A, B]$  and  $\Sigma[A, B]$  measures are constructed from the second moments  $\langle A^2 \rangle$ ,  $\langle B^2 \rangle$ , and  $\langle AB \rangle$  of two extensive quantities  $A$  and  $B$ .

3. A special procedure, the identity method, should be used to calculate the chemical fluctuations in a case of the incomplete particle identification. It solves the misidentification problem for the second and higher moments. Thus the joint multiplicity distribution of particles of different types (a number of species  $k \geq 2$ ) can be uniquely reconstructed.

4. The van der Waals equation of state is considered in the GCE, and particle number fluctuations are calculated. The scaled variance  $\omega[N]$  diverges at the critical point. Admitting a presence of metastable states, one observes that the scaled variance  $\omega[N]$  diverges also at the boundary between the metastable and unstable regions, where  $\partial p / \partial n = 0$ .

**Acknowledgements.** This work was supported by the Humboldt Foundation and by the Program of Fundamental Research of the Department of Physics and Astronomy of National Academy of Sciences, Ukraine

## References

- [1] V. Koch, in *Relativistic Heavy Ion Physics*, Landolt-Börnstein Volume I/23, edited by R. Stock (Springer, Berlin, 2010).
- [2] M. Gazdzicki, M. I. Gorenstein, and P. Seyboth, *Int. Journ. Mod. Phys. E* **23**, 1430008 (2014).
- [3] M. Gazdzicki, M. I. Gorenstein and S. Mrowczynski, *Phys. Lett. B* **585**, 115 (2004).
- [4] M. I. Gorenstein, M. Gazdzicki and O. S. Zozulya, *Phys. Lett. B* **585**, 237 (2004).
- [5] I. N. Mishustin, *Phys. Rev. Lett.* **82**, 4779 (1999); *Nucl. Phys. A* **681**, 56c (2001); H. Heiselberg and A. D. Jackson, *Phys. Rev. C* **63**, 064904 (2001).
- [6] M. Stephanov, K. Rajagopal, and E. Shuryak, *Phys. Rev. Lett.* **81**, 4816 (1998); *Phys. Rev. D* **60**, 114028 (1999); M. Stephanov, *Acta Phys. Polon. B* **35**, 2939 (2004).
- [7] V. Koch, A. Majumder and J. Randrup, *Phys. Rev. Lett.* **95**, 182301 (2005).
- [8] V. Koch, A. Majumder and J. Randrup, *Phys. Rev. C* **72**, 064903 (2005).
- [9] J. Cleymans, H. Oeschler, K. Redlich, and S. Wheaton, *Phys. Rev. C* **73**, 034905 (2006).
- [10] F. Becattini, J. Manninen, and M. Gaździcki, *ibid.* **73**, 044905 (2006).
- [11] A. Andronic, P. Braun-Munzinger, and J. Stachel, *Nucl. Phys. A* **772**, 167 (2006).

- [12] F. Becattini, Z. Phys. C **69**, 485 (1996).
- [13] F. Becattini and U. Heinz, Z. Phys. C **76**, 269 (1997).
- [14] J. Cleymans, K. Redlich, and E. Suhonen, Z. Phys. C **51**, 137 (1991).
- [15] M.I. Gorenstein, M. Gaździcki, and W. Greiner, Phys. Lett. B **483**, 60 (2000).
- [16] M.I. Gorenstein, A.P. Kostyuk, H. Stöcker, and W. Greiner, Phys. Lett. B **509**, 277 (2001).
- [17] F. Becattini and L. Ferroni, Eur. Phys. J. C **35**, 243 (2004); **38**, 225 (2004).
- [18] V.V. Begun, L. Ferroni, M.I. Gorenstein, M. Gaździcki, and F. Becattini, J. Phys. G **32**, 1003 (2006);
- [19] F. Becattini and L. Ferroni, Eur. Phys. J. C **51**, 899 (2007); **52**, 597 (2007).
- [20] Yu.B. Rumer and M.Sh. Ryvkin, *Thermodynamics, Statistical Physics, and Kinetics*, Nauka, 1972 (in Russian).
- [21] K.B. Tolpygo, *Thermodynamics and Statistical Physics*, Kiev University, 1966 (in Russian).
- [22] M. I. Gorenstein, J. Phys. G **35**, 125102 (2008).
- [23] V.V. Begun, M. Gaździcki, M.I. Gorenstein, and O.S. Zozulya, Phys. Rev. C **70**, 034901 (2004).
- [24] V.V. Begun, M.I. Gorenstein, and O.S. Zozulya, Phys. Rev. C **72**, 014902 (2005).
- [25] A. Keränen, F. Becattini, V.V. Begun, M.I. Gorenstein, and O.S. Zozulya, J. Phys. G **31**, S1095 (2005).
- [26] F. Becattini, A. Keränen, L. Ferroni, and T. Gabbriellini, Phys. Rev. C **72**, 064904 (2005).
- [27] J. Cleymans, K. Redlich, and L. Turko, Phys. Rev. C **71**, 047902 (2005); J. Phys. G **31**, 1421 (2005).
- [28] V.V. Begun and M.I. Gorenstein, Phys. Rev. C **73**, 054904 (2006).
- [29] V.V. Begun, M.I. Gorenstein, A.P. Kostyuk, and O.S. Zozulya, Phys. Rev. C **71**, 054904 (2005).
- [30] V.V. Begun, M.I. Gorenstein, A.P. Kostyuk, and O.S. Zozulya, J. Phys. G **32**, 935 (2006).
- [31] V.V. Begun, M.I. Gorenstein, M. Hauer, V.P. Konchakovski, and O.S. Zozulya, Phys. Rev. C **74**, 044903 (2006).
- [32] V.V. Begun, M. Gaździcki, M.I. Gorenstein, M. Hauer, B. Lungwitz, and V.P. Konchakovski, Phys. Rev. C **76**, 024902 (2007).
- [33] M. Hauer, V.V. Begun, and M.I. Gorenstein, Eur. Phys. J. C **58**, 83 (2008).
- [34] M. Hauer, Phys. Rev. C **77**, 034909 (2008).
- [35] J. Rafelski and M. Danos, Phys. Lett. B **97**, 279 (1980).
- [36] B. Lungwitz et al. (NA49 Collaboration), PoS CFRNC2006, 024 (2006); nucl-ex/0610046.
- [37] M.I. Gorenstein and M. Hauer, Phys. Rev. C **78** 041902(R) (2008).
- [38] V.V. Begun, M. Gaździcki, and M.I. Gorenstein, Phys. Rev. C **78**, 024904 (2008).
- [39] M. Gaździcki [NA61/SHINE Collaboration], J. Phys. G **36**, 064039 (2009).
- [40] G. Odyniec [STAR Collaboration], J. Phys. G **35**, 104164 (2008).
- [41] V. P. Konchakovski, M. I. Gorenstein, E. L. Bratkovskaya, and W. Greiner, J. Phys. G **37**, 073101 (2010).
- [42] M. I. Gorenstein and M. Gaździcki, Phys. Rev. C **84**, 014904 (2011).

- [43] M. Gazdzicki, M. I. Gorenstein, and M. Mackowiak-Pawlowska, *Phys. Rev. C* **88**, 024907 (2013).
- [44] M. Gaździcki and St. Mrowczyński, *Z. Phys. C* **54**, 127 (1992).
- [45] E. Sangaline, arXiv:1505.0026 [nucl-th].
- [46] S. A. Bass *et al.*, *Prog. Part. Nucl. Phys.* **41**, 255 (1998);  
M. Bleicher *et al.*, *J. Phys. G* **25**, 1859 (1999).
- [47] K. Grebieszkow, *Acta Phys. Polon. B* **43**, 1333 (2012).
- [48] V. V. Begun, V. P. Konchakovski, M. I. Gorenstein and E. Bratkovskaya, *J. Phys. G* **40**, 045109 (2013).
- [49] M. I. Gorenstein and K. Grebieszkow, *Phys. Rev. C* **89**, 034903 (2014).
- [50] M. I. Gorenstein and M. Rybczynski, *Phys. Lett. B* **730**, 70 (2014).
- [51] T. Anticic *et al.* [NA49 Collaboration], *Phys. Rev. C* **79**, 044904 (2009).
- [52] P. Seyboth [NA49 and NA61/SHINE Collaborations], Proceedings Contribution arXiv:1402.4619; see also slides at <https://atlaswww.hep.anl.gov/ismd13/>.
- [53] T. Czopowicz [NA61/SHINE Collaboration], arXiv:1503/0161; PoS (CPOD-2014).
- [54] V. V. Begun, M. I. Gorenstein, and K. Grebieszkow, arXiv:1409.3023[nucl-th], *J. Phys. G*, in print.
- [55] S. Jeon and V. Koch, *Phys. Rev. Lett.* **83**, 5435 (1999).
- [56] M. Gazdzicki, *Eur. Phys. J. C* **8**, 131 (1999).
- [57] M. Gazdzicki, K. Grebieszkow, M. Maćkowiak, and S. Mrówczyński, *Phys. Rev. C* **83**, 054907 (2011).
- [58] M. I. Gorenstein, *Phys. Rev. C* **84**, 024902 (2011).
- [59] A. Rustamov and M.I. Gorenstein, *Phys. Rev. C* **86**, 044906 (2012).
- [60] A. Stephanov, *Phys. Rev. Lett.* **102**, 032301 (2009); **107**, 052301 (2011).
- [61] C. Athanasiou, K. Rajagopal, and M. Stephanov, *Phys. Rev. D* **82**, 074008 (2010).
- [62] T. Anticic *et al.* [NA49 Collaboration], *Phys. Rev. C* **89**, 054902 (2014).
- [63] M. Mackowiak-Pawlowska [NA49 and NA61/SHINE Collaborations], PoS (CPOD 2013), 048;  
M. Mackowiak-Pawlowska and A. Wilczek, arXiv:1402.0707 [hep-ph].
- [64] W. Greiner, L. Neise, and H. Stöcker *Thermodynamics and Statistical Mechanics*, 1995  
Springer-Verlag New York, Inc.
- [65] L. D. Landau and E. M. Lifshitz, *Statistical Physics* (Oxford: Pergamon) 1975.
- [66] V. Vovchenko, D. V. Anchishkin, and M. I. Gorenstein, arXiv:1501.0378[nucl-th].
- [67] M. I. Gorenstein, M. Hauer, and D. O. Nikolajenko, *Phys. Rev. C* **76**, 024901 (2007).